Influence of electronic irradiations on the chemical and structural properties of PEEK for space applications

Guilhem Rival, Thierry Paulmier, Eric Dantras

Influence of electronic irradiations on the chemical and structural properties of PEEK for space applications

G. Rival [a, b], T. Paulmier [a], E. Dantras [b, *]

[a] ONERA - DPHY, The French Aerospace Lab, F-31055, Toulouse, France
[b] CIRIMAT - Université Toulouse III Paul Sabatier, Physique des Polymères, 118 route de Narbonne, 31062, Toulouse, France

ARTICLE INFO

Keywords:
Dynamic mechanical analysis
Ionising radiations
PEEK
Thermal analysis
Thermoplastic polymer

ABSTRACT

Polymer materials used in satellite manufacturing are exposed to severe environmental conditions. Irradiation by high-energy electrons induces chemical modifications of macromolecules. PolyEtherEtherKetone (PEEK) is used in space industry and therefore, its behaviour regarding electronic irradiations has to be studied. Thus, the aim of this work is to investigate the effect of experimental electronic irradiations on the physical and chemical structure of PEEK. In this way, PEEK films were irradiated under high vacuum by a mono-energetic electron beam. Doses deposited are representatives of 15 years in geostationary electronic environment. The study of irradiated samples revealed modifications of the chemical and physical structures. Irradiation predominantly induces cross-linking phenomena in the amorphous phase in front of chain scission phenomena. Irradiation also leads to a decrease in crystallite size and crystallinity ratio.

1. Introduction

In Geostationary Earth Orbit (GEO) environment, satellites' materials are subject to several constraints like micrometeorites, space debris impacts, thermal cycling and irradiations by energetic particles (neutrons, protons, electrons …). In the case of polymer materials, electronic irradiations are responsible for two major issues: charge phenomena and physico-chemical ageing. Since polymer materials are electrical insulators, low-energy electrons are accumulated on their surface. This accumulation leads to an increase in surface electric potential and therefore to electrostatic discharge phenomena which are at the origin of many spacecraft failures [1]. Moreover, irradiation by high-energy electrons induces modifications of the polymer physico-chemical structure which leads to evolution of its initial properties. These phenomena have already been investigated in several studies like Roggero et al. who studied the effect of electronic irradiation on a space-used silicone elastomer [2,3].

PolyEtherEtherKetone (PEEK) is a high performance polymer which is increasingly used for structural application in satellite manufacturing. Because of these new uses, it becomes necessary to investigate PEEK behaviour towards electronic irradiations. Since its first commercialisation by Imperial Chemical Industries in 1978, numerous studies have focused on the behaviour of PEEK and its composites under different radiation sources like gamma rays [4,5], ultraviolet light [6] or under combined ageing [7,8]. In the specific case of electronic irradiations, Sasuga et al. studied the mechanical behaviour evolution of irradiated samples [9,10]. They observed an overall deterioration of tensile properties, amplified in amorphous samples, and an increase in the viscoelastic transition temperature associated with reticulation of amorphous phase. This increase is observed as well by dielectric measurements which also brought into evidence a wider relaxation time distribution [11]. More recently, Kornacka et al. investigated the effect of electronic irradiations on PEEK in order to identify radical compounds formed during ageing [12]. They also observed a decrease in thermal stability. However, they did not show any evolution of Differential Scanning Calorimetry thermograms probably because of the very low dose deposited in their samples.

This paper aims to determine, through various experimental analyses, the influence of electronic irradiations on the physical and chemical structures of PolyEtherEtherKetone. All previous studies were carried out in an oxidative atmosphere which is not representative of space environment. In that way, PEEK samples were irradiated by an electron beam at room temperature but most importantly under high vacuum in order to better represent

* Corresponding author.
E-mail address: eric.dantras@univ-tlse3.fr (E. Dantras).

https://doi.org/10.1016/j.polymdegradstab.2019.108943

satellite environment. Moreover, the doses deposited in samples for this study are representatives of satellite lifetime and of geostationary electronic environment.

2. Materials and methods

2.1. Material

For this study, two types of PEEK films have been used: first one is a high-crystallinity sample of 100 μm in thickness and second one is a low-crystallinity sample with a thickness of 75 μm. The crystallinity ratio of pristine samples have been determined in both cases by Differential Scanning Calorimetry and obtained values are reported in Table 1.

2.2. Experimental simulation of the space environment

To simulate the effects of electronic radiations, samples have been exposed at room temperature and under high vacuum to a mono-energetic electron beam of 350 keV, thanks to SIRENE facility (ONERA, Toulouse, France). Three experimental irradiation campaigns have been carried out. The resulting doses are: 1.2×10^7 Gy and 3.4×10^7 Gy for high-crystallinity samples, 1.4×10^7 Gy for low-crystallinity samples. They were achieved in less than 60 h thanks to the high beam currents (up to 60 nA.cm^{-2}), which represents an average dose rate of 250 Gy.s^{-1} in these conditions and for this material. In the case of low-crystallinity samples, irradiations have been achieved in order to evaluate the influence of the polymer physical structure. Thus, doses higher than 1.4×10^7 Gy were not necessary: this first dose level were sufficient to already notice differences.

These experimental doses D have been calculated using equation (1).

$$D\left(Gy = J.kg^{-1}\right) = 1.6\ 10^{-9} \times \Phi \frac{1}{\rho}\left(\frac{dE}{dx}\right) \quad (1)$$

Where Φ is the total fluence applied during irradiation (cm^{-2}), ρ the material density (g.cm^{-3}) and dE/dx the stopping power (keV.μm^{-1}). This last quantity is defined as the energy lost per unit length by an incident particle passing through a medium. It depends mainly on medium density, its atomic composition and incident particles energy. When normalised by density, it is referred to a mass stopping power usually expressed in MeV.cm^2.g^{-1}.

For this study, electronic stopping power of PEEK was estimated by using the open-source software CASINO ("monte CArlo SImulation of electroN trajectory in sOlids") [13,14]. This software allows performing Monte-Carlo simulations of electron interactions with a system of solids defined by their chemical composition and density. For the sake of simplicity, PEEK was modelled by a carbon solid with a density of 1.3 g.cm^{-3} given by the supplier. Thus, stopping powers resulting from the irradiation by 350 keV electrons were simulated for experimental conditions. Corresponding dose depth profiles, calculated by equation (1), are represented by dashed lines in Fig. 1.

To compare with these experimental profiles, dose deposited by geostationary electronic environment have been calculated as well. For this purpose, the geostationary electron model IGE-2006 was used as basis for calculation [15]. This model gives the energy distribution of electron fluxes φ (keV^{-1}.cm^{-2}.s^{-1}.sr^{-1}) in geostationary orbit. Thus, CASINO simulations of stopping power were performed by varying electron energy over the range [1 keV; 1 MeV]. In addition, a log-log interpolation of the IGE data was made in order to have a higher number of (E, φ) coordinates. Using these simulated data, omnidirectional dose rates (Gy.s^{-1}. sr^{-1}) were calculated for each micrometers of sample by integrating over energy the product of flux φ and mass stopping power. Considering the exposure of a planar surface, dose rate (Gy.s^{-1}) was obtained by multiplying by a factor 2π corresponding to the solid half-angle. Finally, doses D are deduced by multiplying dose rate and exposure time. They are represented by solid lines for 1, 5 and 15 years in Fig. 1.

Fig. 1 shows an homogeneous experimental energy deposition in sample with a ratio between back and front face close to 1.5. This homogeneity is permitted by the high-energy beam which goes through samples without inducing electron implantation. In the case of simulated electronic geostationary environment, profiles show an heterogeneous dose deposition over the sample thickness induced by the distribution of fluxes as described by IGE-2006 model.

According to these simulated data, experimental doses correspond to 15 years of exposure in GEO at a depth of 37 μm ($D = 1.2 \times 10^7$ Gy), 27 μm ($D = 1.4 \times 10^7$ Gy) and 17 μm ($D = 3.4 \times 10^7$ Gy), denoting an acceleration factor higher than 1000 in both cases.

2.3. ThermoGravimetric analysis

In order to investigate evolutions of the polymer thermal stability after irradiation, ThermoGravimetric Analyses (TGA) were performed on a Q50 device from TA Instruments. Samples, placed in oxidising atmosphere (synthetic air) or inert atmosphere (nitrogen), were heated from room temperature to 900 °C at a rate of 20 °C.min^{-1}.

2.4. Differential Scanning Calorimetry

For this study, Differential Scanning Calorimetry (DSC) thermograms were carried out on a DSC 7 manufactured by PerkinElmer. Samples were directly cut from virgin and irradiated sheets for a total analysed mass between 5 and 15 mg. Analysis, carried out under nitrogen flow, consists of two heating runs and one cooling

Table 1
Transitions temperatures, heat capacity jumps and crystallinity ratios of samples as a function of doses. 1st refers to first heating runs and 2nd to second heating runs.

	T_g (°C)		ΔC_p (J.g^{-1}.°C^{-1})		T_m (°C)		χ_c (%)		T_{cc} (°C)	T_c (°C)
	1st	2nd	1st	2nd	1st	2nd	1st	2nd		
High Crystallinity										
Pristine	158	147	0.15	0.14	339	339	34.1	40.1	∅	297
Irradiated 12 MGy	157	150	0.11	0.12	331	333	32.6	33.7	∅	286
Irradiated 34 MGy	159	153	0.16	0.16	318	320	25.8	23.0	∅	269
Low Crystallinity										
Pristine	144	148	0.29	0.13	338	339	13.0	32.2	172	292
Irradiated 14 MGy	147	153	0.30	0.13	318	323	7.6	26.3	185	268

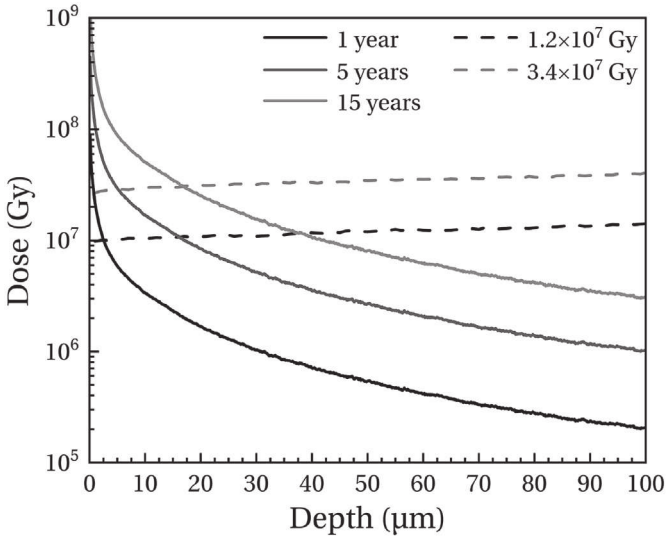

Fig. 1. Dose depth profiles in high-crystallinity PEEK samples (———) and for different exposure times to the geostationary orbit electronic environment (———).

run between 50 °C and 400 °C at a constant rate of 10 °C.min^{-1}. First order transition temperatures are taken at the maximum of the peak while the glass transition temperatures T_g are determined by the tangent method as well as the heat capacity jumps ΔC_p. Crystallinity ratio χ_c of samples was calculated from melting and cold crystallisation enthalpies using equation (2).

$$\chi_c = \frac{\Delta H_m - \Delta H_{cc}}{\Delta H_\infty} \times 100 \quad (2)$$

Where ΔH_m is the sample melt enthalpy (J.g^{-1}), ΔH_{cc} is the cold crystallisation enthalpy (J.g^{-1}) and ΔH_∞ is the theoretical melt enthalpy of a fully crystalline sample determined for PEEK at 130 J.g^{-1} [16].

2.5. Acetone absorption test

To investigate the effect of structural evolution induced by irradiations, acetone (selected penetrant) absorption tests were performed on pristine and irradiated PEEK samples. In the case of using water as penetrant, only a small amount can be absorbed by PEEK (in the order of 0.5 %$_m$ [17,18]) which leads to greater measurement uncertainties. For acetone, Stober and Seferis reported a weight gain of about 7 %$_m$ allowing to minimise uncertainties [19].

Experimentally, samples were dried in a desiccator (under vacuum and with silica gel) during 1 week. Thereafter, they were weighed in order to determine their initial dried mass noted m_0 and then immersed in an acetone bath maintained at room temperature. To carry out the weighing, samples are taken out of the bath, quickly dried with absorbent paper, weighed on a precision balance and then immersed again in acetone. The weight gain (WG) is then calculated by equation (3).

$$WG = \frac{m - m_0}{m_0} \times 100 \quad (3)$$

However, it is well known that due to the density and the low mobility of crystalline phase, absorption phenomena in polymer take place in the amorphous phase. Therefore, in order to take into account a possible crystallinity ratio evolution in irradiated samples, the weight gain will be normalised by the quantity of amorphous phase. The normalised weight gain (NWG) is then calculated with equation (4).

$$NWG = \frac{m - m_0}{(1 - \chi_c/100) \times m_0} \times 100 \quad (4)$$

Where χ_c is the crystallinity ratio (%) calculated from Differential Scanning Calorimetry analyses.

2.6. Dynamic Mechanical Analysis

Dynamic Mechanical Analysis (DMA) tests presented in this study were performed on an ARES G2 strain-controlled rheometer from TA Instruments. Sample dimensions are 35 mm × 12.5 mm. Due to their thickness, PEEK films were analysed in tensile geometry mode to ensure a good signal-to-noise ratio. For each sample, heating runs are performed over the temperature range [-130 °C; 220 °C] at a heating rate of 3 °C.min^{-1}. In order to stay within the material linearity range, strain and frequency were respectively fixed at 0.01% (0.07% for low-crystallinity samples) and 1 Hz allowing the determination of storage $E'_\omega(T)$ and loss $E''_\omega(T)$ moduli.

3. Results and discussion

3.1. Thermal stability of pristine and irradiated samples

Fig. 2-(a) and 2-(b) present the TGA thermograms obtained respectively under nitrogen atmosphere and under air atmosphere for high-crystallinity samples. The top data show the normalised weight m/m_0 while the bottom data show the Derivative ThermoGravimetric (DTG) curves. Since the TGA thermograms of low-crystallinity samples present the same degradation behaviour and the same evolutions after irradiations than high-crystallinity samples, for purpose of clarity they are not presented here.

Under nitrogen or air atmosphere, an intense degradation phenomenon is observed with a maximum intensity at around 600 °C. Vasconcelos et al. [20] associated this degradation with random chain scissions between aromatic cycles and ether or ketone bonds independently of the atmosphere. Under oxidising conditions, a second degradation phenomenon is present, leading to a complete decomposition of sample, which results from oxidation of the first degradation residue. This last degradation seems to occur in three manifestations, respectively at around 650 °C, 675 °C and 700 °C. However, they have not been associated with specific degradation phenomena and literature does not report their origins.

Irradiated samples show an overall decline of their thermal stability. Under nitrogen atmosphere, the temperature position of peak maximum and peak intensity of the primary degradation decrease with an increasing dose which is consistent with the study of Kornacka [12]. An increase in the peak width with dose is also observed. In the case of oxidising atmosphere, same observation can be made despite a peak intensity no longer proportional to dose. These evolutions imply that irradiations necessarily induce chemical modifications of the polymer. Moreover, irradiated sample thermograms performed under air show a new degradation phenomenon near 550 °C. This new peak has been associated with short polymer chains created during irradiation and which degrade at lower temperatures. It indicates that chain scission phenomenon occurs during irradiations. This observation confirms the presence of chemical modifications. Finally, the last degradation phenomenon shows different evolutions after irradiation: an amplification of the two first steps of the degradation and a disappearance of the third one. In the case of the highest dose, a new step can also be observed at higher temperature (around 725 °C). These observations are an additional evidence that irradiations induce chemical

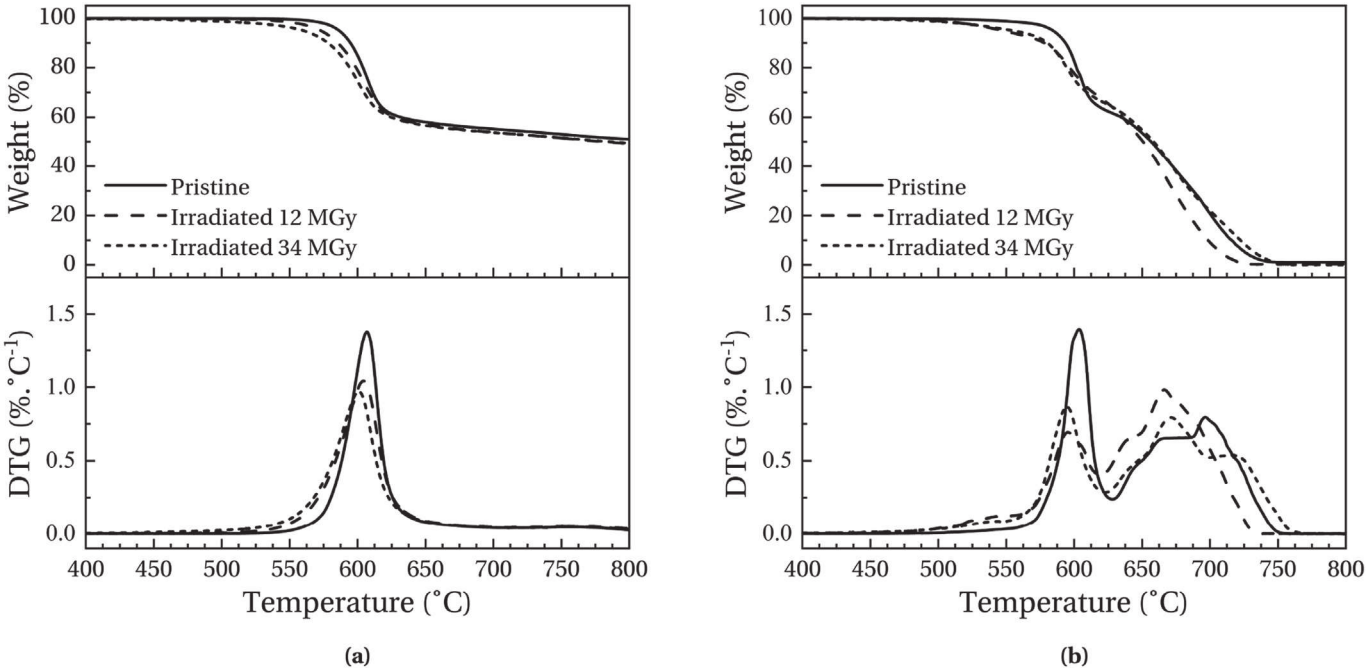

Fig. 2. TGA thermograms, under inert atmosphere **(a)** and under oxidising atmosphere **(b)**, of high-crystallinity samples for the different doses.

modifications. However, due to the poor understanding of the degradation mechanism steps, any further interpretations of these evolutions would not be reliable.

3.2. Physico-chemical structure evolutions

Fig. 3-(a) and 3-(b) present respectively the evolution of heating and cooling thermograms with the dose for high-crystallinity samples. Thermal transition parameters extracted from the analysis of these curves are reported for both physical structures as a function of dose in Table 1.

For the pristine sample, a glass transition temperature of 158 °C is measured during the first heating run. On the second heating run, T_g decrease of almost 10 °C. This phenomenon has been associated with internal stresses induced by manufacturer during film processing and which relax during the first run. Finally, between 1st and 2nd heating run, an increase in the crystallinity ratio χ_c is observed. This evolution is associated with the presence of a shoulder below the melting peak on the 2nd heating run thermograms. This phenomenon is due to secondary crystallisation which is well documented for the PolyArylEtherKetone polymer family [21,22].

Irradiated sample thermograms show significant evolutions after irradiations.

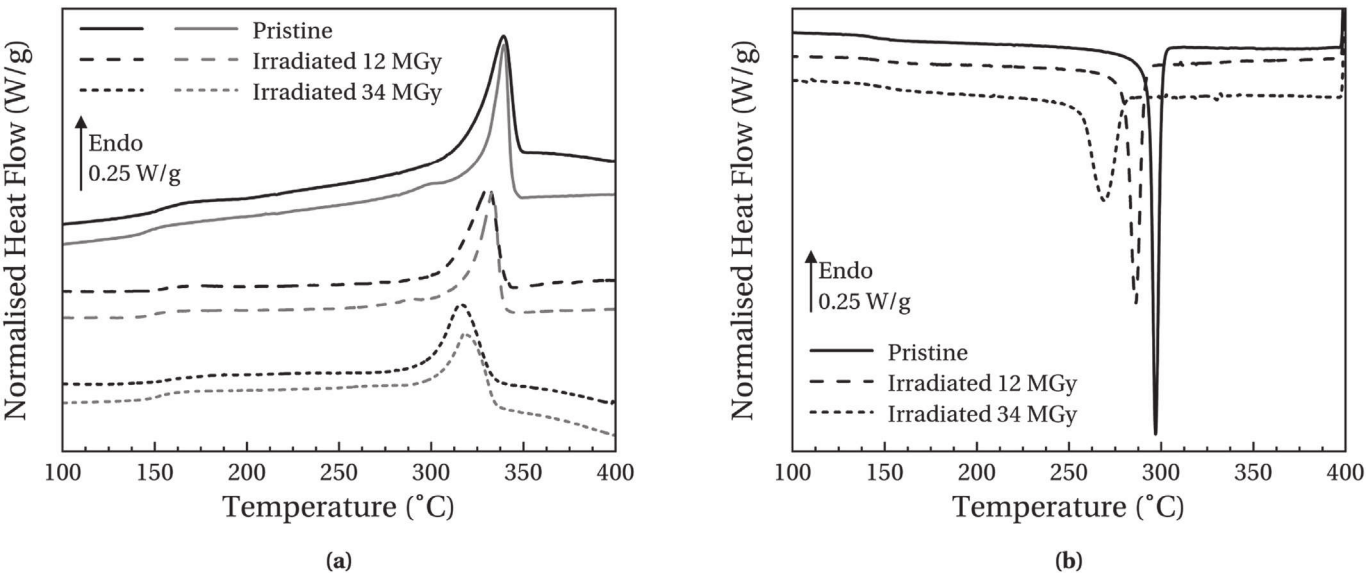

Fig. 3. Heating thermograms **(a)** and cooling thermograms **(b)** of high-crystallinity samples as a function of dose. First heating runs are represented in black lines and second heating runs in grey lines.

- Second heating runs shows that T_g increase by 6 °C (cf. Table 1) for a dose of 34 MGy. This shift to higher temperatures is linked to a decrease in macromolecules mobility which is often related to cross-linking. Moreover, the crystallisation temperature T_c measured during the cooling run shifts to lower temperatures with the dose. This is consistent with a cross-linking phenomenon which induces slower crystallisation kinetics: in the melting state, cross-links limit the reorganisation of polymer chains in crystallites. A broadening of the crystallisation peak is also observed with an increasing dose which is indicative of a more heterogeneous medium after irradiation and leads to a greater distribution of crystallisation kinetics.
- Melting temperature T_m measured during the first heating run (339 °C for pristine sample) decreases significantly with the dose: about 20 °C for the highest dose. This shift is associated with less stable crystalline entities which require less energy to melt. Thus, irradiations decrease the stability of the crystalline phase by creating defects in it. Moreover, the crystallinity ratio decreases as well in irradiated samples. This observation suggests that the created defects lead to a decrease in crystallite size. This hypothesis is confirmed by Yoda which observed by X-Ray Diffraction an average decrease of 15% in crystallite size in electron-irradiated PEEK samples [23]. Furthermore, a broadening of the melting peak is observed with ageing which indicates that irradiations also increase the crystallite size distribution.
- Finally, the decrease in T_m and χ_c during the second run confirms the chemical nature of observed modifications. Indeed, even after passing by the molten state, samples do not recover their initial state. Furthermore, irradiations limit the secondary crystallisation phenomenon observed during the second heating run: $\Delta\chi_c$ value between first and second heating run decreases in irradiated samples and even becomes negative for the highest ageing.

Fig. 4-(a) and 4-(b) present respectively heating and cooling thermograms of low-crystallinity pristine and irradiated samples.

During the first heating run, a cold crystallisation peak is observed at a temperature T_{cc} of 172 °C for the pristine sample. Moreover, a glass transition temperature of 144 °C is measured during this run. This lower value compared to high-crystallinity samples can be explained by a decrease in rigid amorphous phase fraction RAF [24,25]. Indeed, lower quantity of crystalline entities induces a lower RAF and therefore, increase the amorphous phase mobility.

- Low-crystallinity irradiated sample shows similar evolutions compared to those of high-crystallinity samples. However, modifications are more significant in low-crystallinity samples. For example, for a similar dose (14 MGy), the glass transition temperature during the second run increases by 5 °C for the low-crystallinity sample and just 3 °C for the high-crystallinity sample. This more significant evolution compared to high-crystallinity samples indicates that the presence of crystallites increases the stability of samples against electronic irradiation. This trend has already been observed by Hegazy et al. who have detected higher gas emissions in amorphous samples than in semi-crystalline samples [26]. Their results corroborate the hypothesis that crystalline phase stabilises samples in the standpoint of cross-linking.
- The evolutions are also more significant in the case of melting temperature. However, the origin of crystalline entities between low and high crystallinity samples is not the same. For high-crystallinity samples, crystallites are present during the irradiation and therefore, the decrease in T_m and χ_c is due to the direct modification of crystallite size. For low-crystallinity samples, the majority of crystallites which melt at T_m on the first heating run appeared during the cold crystallisation. Thus, the decrease in T_m is mainly due to a limited cold crystallisation phenomenon induced by the cross-linking of macromolecules. This is confirmed by the increase in cold crystallisation temperature and the decrease in ΔH_{cc}. The values of ΔH_{cc} are not reported in the table but decrease from 23 $J.g^{-1}$ in pristine sample to 20 $J.g^{-1}$ in irradiated sample. Furthermore, the cold crystallisation peak broaden after irradiation indicating an increase in the medium heterogeneity. Finally, the value of χ_c measured during the first heating run decrease with an increasing ionising dose. This behaviour is the same than in high-crystallinity sample. Since equation (2) takes into account cold crystallisation, this decrease is due to the direct damaging of crystallites during irradiation.

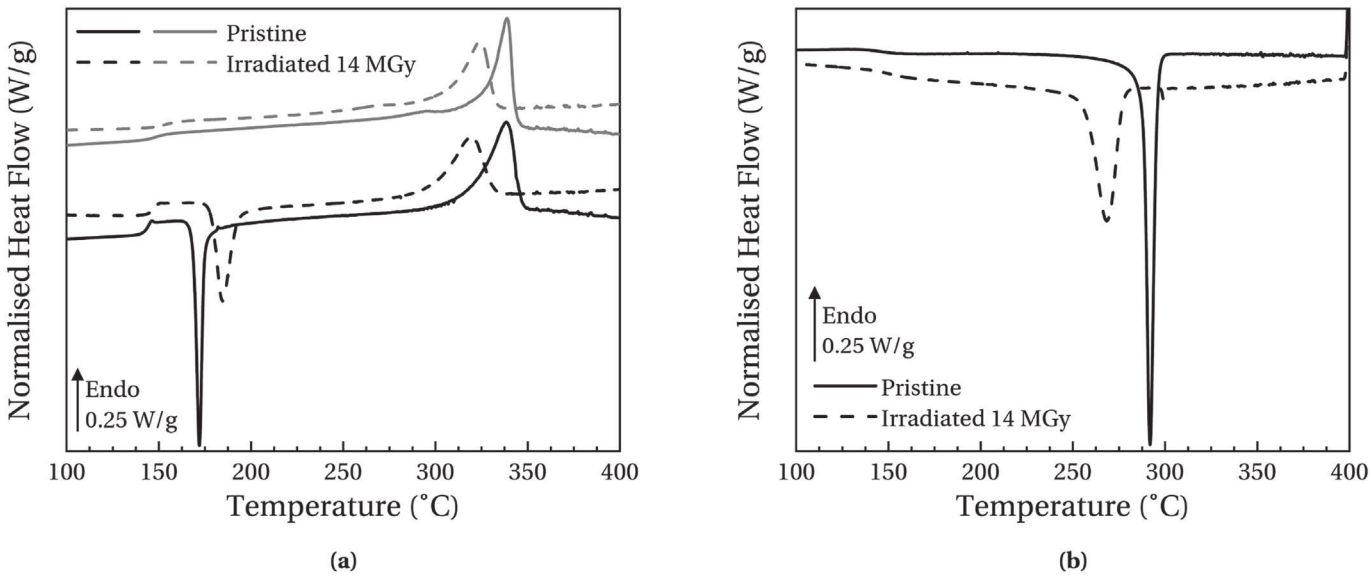

Fig. 4. Heating thermograms **(a)** and cooling thermograms **(b)** of low-crystallinity samples as a function of dose. First heating runs are represented in black lines and second heating runs in grey lines.

These evolutions of physical and chemical structures are analogous to those observed by Hegazy et al. in the case of amorphous and semi-crystalline PEEK samples subjected to γ irradiations under vacuum [5]. In their study, they also associated these evolutions with cross-linking of amorphous phase. Thus, ageing mechanisms under electronic irradiations or under γ irradiations look to be the same.

3.3. Evidence of cross-linking through absorption tests

Fig. 5 shows the normalised acetone weight gain as a function of immersion time for low-crystallinity and high-crystallinity samples. In order to highlight any evolutions for high-crystallinity samples, swelling tests were carried out only for the highest dose.

Some qualitative observations can be made from data in Fig. 5. Whether for pristine or irradiated samples, mass uptake shows faster absorption kinetics and higher equilibrium weight gain m_∞ for low-crystallinity samples. Indeed, several studies have observed this behaviour in polymer systems [27,28]. It has been linked with the fact that only the amorphous phase can absorb penetrants. Indeed, the higher density of crystalline phase limits absorption phenomena. Thus, with an increasing amorphous phase ratio the quantity of penetrant which can be absorbed increases but also, its diffusion through the polymer is fastest due to less crystallites. In the case of PEEK, this behaviour has been observed as well by Stober and Seferis with methylene chloride [19].

After irradiation, faster absorption kinetics are observed in both physical structures. This evolution has been associated with the decrease in crystallinity observed in irradiated samples by DSC analysis. Indeed, the quantity of crystalline entities being lower, the penetrant diffusion is easier and therefore, the absorption rate increases. Regarding the value of equilibrium weight gain, a decrease is observed after irradiation for the low-crystallinity sample. First of all, it can be expected that the decrease in sample crystallinity should have induced a higher equilibrium weight gain as observed in pristine samples. This opposite evolution indicates that another parameter affects its value. Thus, it can be explained by the cross-linking of macromolecules which decreases the maximum fraction of penetrant that can be absorbed by the amorphous phase. Indeed, the presence of cross-links limits the swelling of the amorphous phase and therefore, decreases the volume available for the penetrant. For high-crystallinity samples, the value of m_∞ is identical before and after irradiation. DSC analysis showed indeed that the presence of crystallites stabilises the amorphous phase. Thus, the effect of cross-linking in the amorphous phase is compensated by a higher $\Delta\chi_c$ between pristine and irradiated samples.

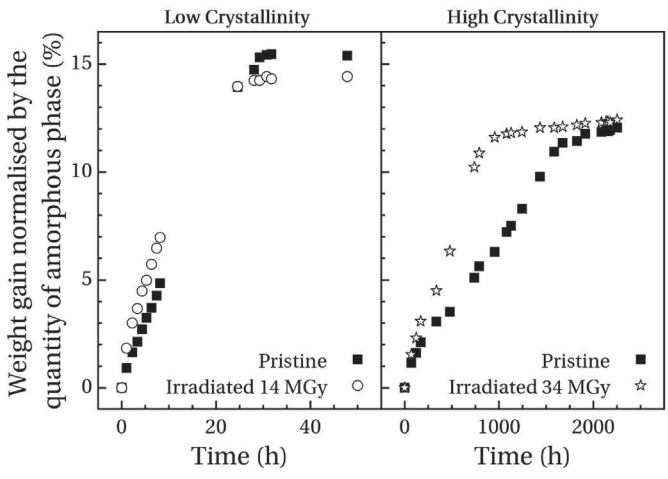

Fig. 5. Evolution with the dose of weight gain kinetics for low-crystallinity samples andhigh-crystallinity samples.

From the analysis of absorption data, the determination of a diffusion coefficient is only possible if the mass uptake follows a Fick's diffusion law. From Alfrey et al. [29], the weight gain m(t) normalised by its equilibrium value m_∞ can be fitted with the following equation:

$$\frac{m(t)}{m_\infty} = Kt^n \tag{5}$$

Where the value of the parameter **n** depends on the absorption mechanism. A value of 1/2 indicates a Fickian diffusion and therefore, the parameter **K** is related to the diffusion coefficient ($cm^2.s^{-1}$) [30]. For a value of 1, the absorption mechanism is referred as Case II diffusion. In this case, parameter **K** can be related to the penetrant front velocity ($cm.s^{-1}$). For a value of n between 0.5 and 1, the diffusion is called anomalous and **K** cannot be associated with any physical parameters. These last two diffusion mechanisms (Case II and anomalous) are often observed when absorption tests are performed below the glass transition temperature [31]. This can be explained by comparing the characteristic time of macromolecules relaxation $\tau_{relax.}$ to the characteristic time of diffusion $\tau_{diff.}$. Indeed, above glass transition temperature, $\tau_{relax.} < \tau_{diff.}$ and therefore, the absorption process is controlled by the diffusion and can be describe by a Fick's law. Below glass transition temperature, $\tau_{relax.} > \tau_{diff.}$ meaning that the process is controlled by macromolecules relaxation which induces a non-Fickian behaviour.

In this study, the fit of $m(t)/m_\infty$ by equation (5) reported in Table 2 gives a value of **n** between 0.5 and 1 for all samples, denoting an anomalous diffusion mechanism. The absorption tests being carried out at a temperature well below the glass transition of PEEK, this behaviour is not surprising but therefore, the determination of a diffusion coefficient is not possible.

Between high and low crystallinity samples, the parameter **K** increases. Indeed, its value is related to diffusion kinetics and, since diffusion processes are faster in amorphous samples, this increase is linked to the decrease in χ_c. Regarding parameter **n**, its value decreases with increasing χ_c. For polymers, anomalous and Case II diffusion mechanisms are related to the presence of amorphous phase. Thus, when the polymer becomes closer to a fully crystalline theoretical state, the diffusion mechanism gets closer to a Fickian behaviour. Moreover, numerous studies have demonstrated that amorphous polymers present Case II behaviour, *i.e.* a parameter **n** equal to 1 like Weisenberger et al. for methanol in PMMA [32] or Qin et al. for acetone in PolyCarbonate [33].

After irradiation, an increase in parameter **K** is observed for both crystallinity ratio. This evolution confirms the faster diffusion kinetics observed on Fig. 5 and which has been associated with the decrease in χ_c. For the parameter **n**, opposite evolutions are

Table 2
Parameters K and n obtained from the fit of $m(t)/m_\infty$ by equation (5) compared to χ_c obtained from 1st heating runs in DSC analysis.

	K (s^{-n})	n	χ_c (%)
High Crystallinity			
Pristine	1.6×10^{-3}	0.85	34.1
Irradiated 34 MGy	2.1×10^{-3}	0.89	25.8
Low Crystallinity			
Pristine	43×10^{-3}	0.95	12.8
Irradiated 14 MGy	120×10^{-3}	0.65	06.5

observed between high and low crystallinity samples. While a little increase is observed for the high-crystallinity samples, an important decrease is observed for amorphised samples: the diffusion process becomes closer to a Fickian behaviour. This could indicates that cross-linking of the amorphous phase limits the influence of chains relaxation on the diffusion process and therefore, leads to a quasi-Fick mechanism. For high-crystallinity samples, the influence of cross-linking could be negligible in front of the increase in amorphous phase quantity and therefore, the diffusion gets closer to a Case II mechanism.

3.4. Influence of irradiations on the mechanical behaviour

Fig. 6 presents the DMA thermograms of high-crystallinity samples, pristine and irradiated.

Loss modulus E″ thermogram of the pristine sample shows two distinct relaxation phenomena. At low temperature, the broad peak at about −90 °C is labelled γ relaxation. It has been associated in the literature with dipolar entities which can interact with water like ketone groups present on the main chain [34,35]. Literature also highlights another secondary relaxation named β, located at around −60 °C, associated with the oscillation of phenyl groups around their axis. However, in elongational strain mode, this relaxation is difficult to point out. At higher temperature, the intense peak near 150 °C corresponds to the viscoelastic relaxation (*i.e.* the mechanical manifestation of the glass transition) also named α relaxation.

Two clear evolutions can be pointed out on the thermograms of irradiated samples. On one hand, an increase in T_α with the dose is observed. Like for the increase in T_g, this indicates that the cross-linking induced by irradiation decreases the macromolecules mobility. This shift to higher temperature is also accompanied with an increase in the width of the viscoelastic relaxation peak. This broadening is attributed to the increase in heterogeneities around relaxing entities responsible of the α relaxation.

On the other hand, a higher rubber modulus value E_{rubber} is observed in irradiated samples. In the rubbery state, the mechanical properties of a thermoplastic polymer are maintained by the presence of crystallites. However, the decrease in crystallinity in irradiated samples observed by DSC should induce a lower E_{rubber}. Thus, this increase can only be explained by a cross-linking phenomenon which limits the mobility of macromolecules on the rubbery plateau.

Moreover, no change in γ relaxation mode is observed, neither on the position nor on the amplitude. This relaxation being associated with a localised macromolecular mobility, this observation indicates that the density of the cross-linking is low and therefore, not sufficient to have a local influence. Thus, the characteristic length between cross-links is smaller than the size of relaxing entities involved in viscoelasticity but larger than those of the γ relaxation. In other words, some relaxing entities involved in γ relaxation are probably modified by the irradiation but their mechanical response are hidden in the response of unmodified entities.

Fig. 7 presents the storage modulus thermogram of low-crystallinity samples before and after irradiation. As for high-crystallinity samples, the modulus drops at almost 150 °C due to the viscoelastic transition. The amplitude of this drop is higher than for high-crystallinity samples due to the lower quantity of crystallites. At higher temperatures, an increase in modulus, symbolised by a rising arrow on the graph, is observed. This behaviour is associated with the cold crystallisation phenomenon. Indeed, the increase in crystallinity limits the mobility of macromolecules and therefore, increases the value of E_{rubber}.

After irradiation, these two phenomena are shifted to higher temperatures which is consistent with DSC analyses. However, the value of E_{rubber} after the cold crystallisation decreases in irradiated sample in contrast to high-crystallinity samples. In this case, crystallites at the origin of samples mechanical resistance were formed during the analysis. Thus, this decrease is the consequence of the limited cold crystallisation which leads to lower crystallinity ratio and therefore, a lower rubber modulus.

4. Conclusion

This work studied, through different experimental approaches, the influence of electronic irradiations on the physical an chemical structures of PolyEtherEtherKetone. In this way, the SIRENE facility installed at ONERA was used to irradiate samples, under high vacuum and at room temperature, with high-energy electrons (350 keV) and with high current beam densities (up to 60 nA.cm^{-2}). Three irradiation campaigns were carried out leading to three average doses: 1.2×10^7 Gy and 3.4×10^7 Gy for the high-crystallinity samples, 1.4×10^7 Gy for the low-crystallinity sample.

DSC analyses revealed that irradiations induced modifications of

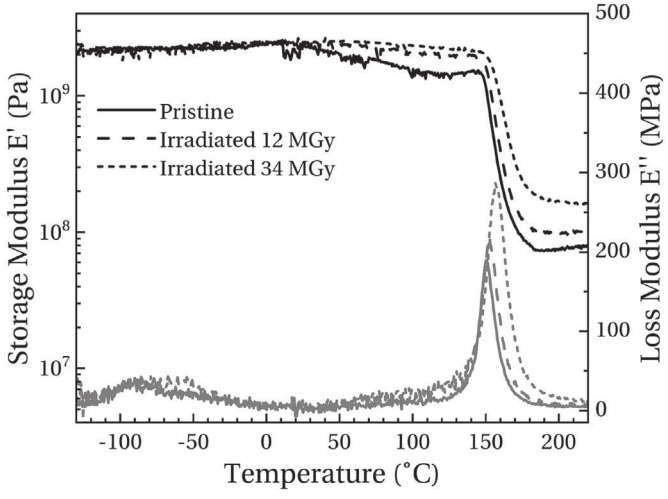

Fig. 6. DMA thermograms of high-crystallinity pristine and irradiated samples. Storage moduli are represented in black lines and loss moduli in grey lines.

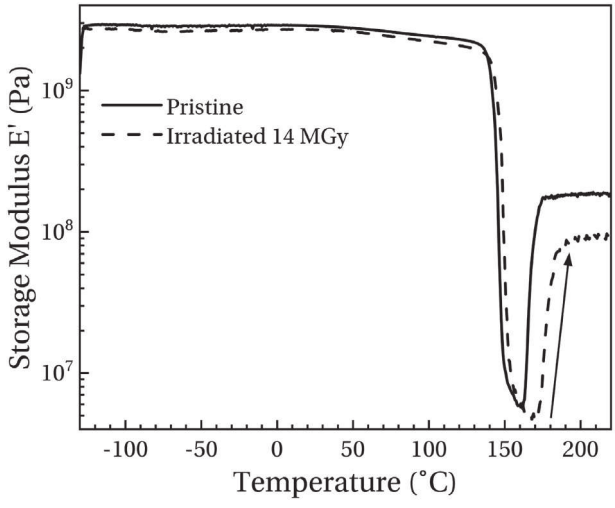

Fig. 7. Storage modulus thermogram of low-crystallinity pristine and irradiated samples.

both physical and chemical structures of PEEK. The decrease in the melting temperature and the crystallinity ratio of high-crystallinity samples has been linked to the decrease in crystallite size during irradiation. In the case of low-crystallinity samples, these decreases are due to a limited cold crystallisation which is also seen through the increase in T_{cc}. This indicates a decrease in macromolecules mobility. Moreover, in both types of samples, an increase in the glass transition temperature has been observed and is consistent with a decrease in mobility. Due to the irreversibility of these modifications revealing their chemical nature, it has been concluded that irradiation induces preponderantly cross-linking of macromolecules. This behaviour has already been observed under γ irradiations [5]. Nonetheless, chain scission phenomenon has also been observed through the degradation of smaller-length chains in TGA.

Through acetone absorption tests, this cross-linking has been highlighted by the decrease in the equilibrium weight gain in low-crystallinity samples. Indeed, cross-links limits the swelling of amorphous phase and therefore, decreases the fraction of penetrant which can be absorb. It has also been shown that the decrease in crystallinity ratio induces an increase in absorption kinetics.

Finally, DMA tests showed that the localised γ relaxation was unmodified after irradiation. This allowed us to conclude that cross-linking density is low. Moreover, an opposite evolution of E_{rubber} has been observed between both physical structures of samples and has been linked to the origin of crystallites responsible of the mechanical behaviour of rubbery plateau.

Acknowledgement

The authors would like to thank the CNES for technical support (funding of the SIRENE facility) and the Région Occitanie for financial support in this project.

References

[1] R.D. Leach, Failures and Anomalies Attributed to Spacecraft Charging, NASA Marshall Space Flight Center, 1995. Tech. Rep. Tech. Rep. NASA-RP-1375.
[2] A. Roggero, E. Dantras, T. Paulmier, C. Tonon, S. Dagras, S. Lewandowski, D. Payan, Inorganic fillers influence on the radiation-induced ageing of a space-used silicone elastomer, Polym. Degrad. Stab. 128 (2016) 126–133.
[3] A. Roggero, E. Dantras, T. Paulmier, C. Tonon, S. Lewandowski, S. Dagras, D. Payan, Electrical conductivity of a silicone network upon electron irradiation: influence of formulation, J. Phys. D Appl. Phys. 49 (2016) 505303.
[4] T. Sasuga, M. Hagiwara, Radiation deterioration of several aromatic polymers under oxidative conditions, Polymer 28 (1987) 1915–1921.
[5] E.-S.A. Hegazy, T. Sasuga, T. Seguchi, Irradiation effects on aromatic polymers: 3. Changes in thermal properties by gamma irradiation, Polymer 33 (1992) 2911–2914.
[6] H. Nakamura, T. Nakamura, T. Noguchi, K. Imagawa, Photodegradation of PEEK sheets under tensile stress, Polym. Degrad. Stab. 91 (2006) 740–746.
[7] G. Ajeesh, S. Bhowmik, V. Sivakumar, L. Varshney, V. Kumar, M. Abraham, Investigation on polyetheretherketone composite for long term storage of nuclear waste, J. Nucl. Mater. 467 (2015) 855–862.
[8] L. Yang, Y. Ohki, N. Hirai, S. Hanada, Aging of poly(ether ether ketone) by heat and gamma rays —— its degradation mechanism and effects on mechanical, dielectric and thermal properties, Polym. Degrad. Stab. 142 (2017) 117–128.
[9] T. Sasuga, N. Hayakawa, K. Yoshida, M. Hagiwara, Degradation in tensile properties of aromatic polymers by electron beam irradiation, Polymer 26 (1985) 1039–1045.
[10] T. Sasuga, M. Hagiwara, Mechanical relaxation of crystalline poly(aryl-ether-ether-ketone) (PEEK) and influence of electron beam irradiation, Polymer 27 (1986) 821–826.
[11] S. Fujita, K. Shinyama, M. Baba, Dielectric properties of electron beam irradiated PEEK, 10th International Symposium on Electrets (ISE 10), in: Proceedings (Cat. No.99 CH36256, 1999, pp. 115–118.
[12] E.M. Kornacka, G. Przybytniak, A. Nowicki, Radical processes initiated by ionizing radiation in PEEK and their macroscopic consequences, Polym. Adv. Technol. 30 (2019) 79–85.
[13] D. Drouin, A.R. Couture, D. Joly, X. Tastet, V. Aimez, R. Gauvin, CASINO V2.42——A fast and easy-to-use modeling tool for scanning electron microscopy and microanalysis users, Scanning 29 (2007) 92–101.
[14] H. Demers, N. Poirier-Demers, A.R. Couture, D. Joly, M. Guilmain, N. de Jonge, D. Drouin, Three-dimensional electron microscopy simulation with the CASINO Monte Carlo software, Scanning 33 (2011) 135–146.
[15] A. Sicard-Piet, S. Bourdarie, D. Boscher, R.H.W. Friedel, M. Thomsen, T. Goka, H. Matsumoto, H. Koshiishi, A new international geostationary electron model: IGE-2006, from 1 keV to 5.2 MeV, Space Weather 6 (2008) S07003.
[16] D.J. Blundell, B.N. Osborn, The morphology of poly(aryl-ether-ether-ketone), Polymer 24 (1983) 953–958.
[17] M.A. Grayson, C.J. Wolf, The solubility and diffusion of water in poly(aryl-ether-ether-ketone) (PEEK), J. Polym. Sci., Polym. Phys. Ed. 25 (1987) 31–41.
[18] G. Mensitieri, A. Apicella, J.M. Kenny, L. Nicolais, Water sorption kinetics in poly(aryl ether ether ketone), J. Appl. Polym. Sci. 37 (1989) 381–392.
[19] E.J. Stober, J.C. Seferis, Fluid sorption characterization of PEEK matrices and composites, Polym. Eng. Sci. 28 (1988) 634–639.
[20] G.d.C. Vasconcelos, R.L. Mazur, B. Ribeiro, E.C. Botelho, M.L. Costa, Evaluation of decomposition kinetics of poly (ether-ether-ketone) by thermogravimetric analysis, Mater. Res. 17 (2013) 227–235.
[21] P. Cebe, S. Hong, Crystallization behaviour of poly(ether-ether-ketone), Polymer 27 (1986) 1183–1192.
[22] L. Quiroga Cortés, N. Caussé, E. Dantras, A. Lonjon, C. Lacabanne, Morphology and dynamical mechanical properties of poly ether ketone ketone (PEKK) with meta phenyl links, J. Appl. Polym. Sci. 133 (2016) 43396.
[23] O. Yoda, The crystallite size and lattice-distortions in the chain direction of irradiated poly (aryl-Ether-Ketone), Polym. Commun. 26 (1985) 16–19.
[24] P. Huo, P. Cebe, Effects of thermal history on the rigid amorphous phase in poly(phenylene sulfide), Colloid Polym. Sci. 270 (1992) 840–852.
[25] S.Z.D. Cheng, M.Y. Cao, B. Wunderlich, Glass transition and melting behavior of poly(oxy-1,4-phenyleneoxy-1,4-phenylenecarbonyl-1,4-phenylene) (PEEK), Macromolecules 19 (1986) 1868–1876.
[26] E.-S.A. Hegazy, T. Sasuga, M. Nishii, T. Seguchi, Irradiation effects on aromatic polymers: 2. Gas evolution during electron-beam irradiation, Polymer 33 (1992) 2904–2910.
[27] L. Perrin, Q.T. Nguyen, R. Clement, J. Neel, Sorption and diffusion of solvent vapours in poly(vinylalcohol) membranes of different crystallinity degrees, Polym. Int. 39 (1996) 251–260.
[28] V. Compañ, L.F. Del Castillo, S.I. Hernández, M.M. López-González, E. Riande, Crystallinity effect on the gas transport in semicrystalline coextruded films based on linear low density polyethylene, J. Polym. Sci., Polym. Phys. Ed. 48 (2010) 634–642.
[29] T. Alfrey, E.F. Gurnee, W.G. Lloyd, Diffusion in glassy polymers, J. Polym. Sci., Polym. Symp. 12 (1966) 249–261.
[30] N.A. Peppas, L. Brannon-Peppas, Water diffusion and sorption in amorphous macromolecular systems and foods, J. Food Eng. 22 (1994) 189–210.
[31] L. Masaro, X. Zhu, Physical models of diffusion for polymer solutions, gels and solids, Prog. Polym. Sci. 24 (1999) 731–775.
[32] L.A. Weisenberger, J.L. Koenig, An NMR imaging study of methanol desorption from partially swollen PMMA rods, Macromolecules 23 (1990) 2454–2459.
[33] W. Qin, Y. Shen, L. Fei, NMR imaging of acetone diffusion process in polycarbonate, Chin. J. Polym. Sci. 11 (1993) 358–363.
[34] J.E. Harris, L.M. Robeson, Miscible blends of poly(aryl ether ketone)s and polyetherimides, J. Appl. Polym. Sci. 35 (1988) 1877–1891.
[35] M. Coulson, L. Quiroga Cortés, E. Dantras, A. Lonjon, C. Lacabanne, Dynamic rheological behavior of poly(ether ketone ketone) from solid state to melt state, J. Appl. Polym. Sci. 135 (2018) 46456.